PAPER

Dosimetric feasibility of intensity modulated proton therapy in a transverse magnetic field of 1.5 T

IOP Publishing | Institute of Physics and Engineering in Medicine Physics in Medicine & Biology

Phys. Med. Biol. **60** (2015) 5955–5969 doi:10.1088/0031-9155/60/15/5955

Dosimetric feasibility of intensity modulated proton therapy in a transverse magnetic field of 1.5 T

J Hartman[1], C Kontaxis[1], G H Bol[1], S J Frank[2], J J W Lagendijk[1], M van Vulpen[1] and B W Raaymakers[1]

[1] Department of Radiotherapy, University Medical Center Utrecht, 3584 CX Utrecht, The Netherlands
[2] Department of Radiation Oncology, The University of Texas MD Anderson Cancer Center, Houston, TX 77030, USA

E-mail: j.hartman@umcutrecht.nl

Received 10 February 2015, revised 5 June 2015
Accepted for publication 18 June 2015
Published 17 July 2015

Abstract

Proton therapy promises higher dose conformality in comparison with regular radiotherapy techniques. Also, image guidance has an increasing role in radiotherapy and MRI is a prime candidate for this imaging. Therefore, in this paper the dosimetric feasibility of Intensity Modulated Proton Therapy (IMPT) in a magnetic field of 1.5 T and the effect on the generated dose distributions compared to those at 0 T is evaluated, using the Monte Carlo software TOol for PArticle Simulation (TOPAS). For three different anatomic sites IMPT plans are generated. It is shown that the generation of an IMPT plan in a magnetic field is feasible, the impact of the magnetic field is small, and the resulting dose distributions are equivalent for 0 T and 1.5 T. Also, the framework of Monte Carlo simulation combined with an inverse optimization method can be used to generate IMPT plans. These plans can be used in future dosimetric comparisons with e.g. IMRT and conventional IMPT. Finally, this study shows that IMPT in a 1.5 T magnetic field is dosimetrically feasible.

Keywords: proton therapy, image-guided radiotherapy, mri-guided, monte carlo simulations

(Some figures may appear in colour only in the online journal)

1. Introduction

Proton therapy is a form of radiotherapy which uses protons, instead of photons or electrons, as in regular radiotherapy. The main difference with photon based radiotherapy, is that a beam of protons stops at a certain depth inside the body. Where the proton beam stops, it will deliver most of its energy, a point known as the Bragg Peak (BP) (Paganetti 2012a). Because of this property, proton therapy treatment promises to deliver a conformal dose to the target, while at the same time decreasing the dose to the organs at risk (OARs) compared with photon-based treatments (Glimelius *et al* 1999, Suit *et al* 2003, Mock *et al* 2004, Trofimov *et al* 2007). To accomplish this benefit, it is crucial to know the exact position of the target. Because of the sharp dose fall-off at the BP, a misalignment of a few millimeters could lead to a decrease of the dose in the target of >80% and an increase of this amount of dose in the surrounding tissue. Also, because of range uncertainty on the proton beam, a margin on the location of the Bragg Peak has to be taken into account (Paganetti 2012b). This is both due to errors in modelling, uncertainty in physics and errors because of CT resolution or conversion to tissue parameters. Therefore, additional margins are introduced leading to larger treatment volumes. Up-to-date imaging of the target and OARs, before and during radiation delivery, is therefore important for the delivery of the optimal plan. Several solutions to provide such image data can be considered, one of which is image-guided radiotherapy (IGRT) (Mackie *et al* 2003). Current clinical proton therapy systems are recently integrated with cone beam CT, such as the systems from IBA, Belgium and Hitachi, Japan.

Currently, robust optimization might be used as a method to manage the uncertainty with regard to the dose delivery in proton therapy (Unkelbach *et al* 2009, Chen *et al* 2012, Liu *et al* 2012), as conventional plans with a geometry-based PTV are sensitive to range uncertainties (Park *et al* 2012). In the robust approach, range and position uncertainties are incorporated in the optimization process, so they are taken into account when calculating the weights of the proton beams (Chen *et al* 2012, Liu *et al* 2012). Compared to a conventional approach with a geometrically expanded PTV, this creates more robust plans (Unkelbach *et al* 2009, Liu *et al* 2013), but with wider margins.

Magnetic Resonance Imaging (MRI) has several advantages when compared with other imaging modalities. It has a superior soft tissue contrast compared with CT, while it does not use ionizing radiation for image formation. The latter allows continuous imaging and also makes it a preferable imaging technique in pediatrics (Brenner and Hall 2007, Semelka *et al* 2007). The superior soft tissue contrast, combined with the possibility of functional imaging, can lead to better tissue characterization (Schepper *et al* 2000) which can potentially be used to more accurately determine stopping powers (Rank *et al* 2013b), improve the delineation of the target (Nguyen *et al* 2013) and thus improve the conformality of the dose delivered to the tumor. The combination of improved determination of stopping powers and the better knowledge of the tumor position, can also lead to the use of smaller margins.

In the case of IGRT, it is favorable to be able to combine the imaging system with the treatment system. Using such a hybrid system, it is possible to (1) perform online imaging to evaluate the position and shape of the clinical target volume, (2) take into consideration the setup errors while the patient is in treatment position on the couch and (3) work towards real-time imaging of the tumor and adapt the beam during treatment. The first two points could adjust the delivered plan for inter-fraction differences, while the third addresses intra-fraction motion, such as breathing, which in the case of proton therapy might have considerable impact on the dose distribution of the target (Unkelbach *et al* 2007, Lomax 2008). To make use of these advantages, an MRI integrated with a linear accelerator (MR-linac) has been described and developed (Raaymakers *et al* 2009). It is currently being installed at the UMC Utrecht,

The Netherlands. The MD Anderson Cancer Center will be the second institute in the world, and the first in the United States, at which the MR-linac will be installed. Similar systems are developed by groups in Australia (Keall *et al* 2014) and Canada (Fallone 2014).

These concepts have led to the consideration of a possible hybrid MRI proton therapy system. However, such a system poses major dosimetric and technical challenges. Protons are charged particles, so they are subject to the Lorentz force when passing through a magnetic field. This will lead to a curved path of the protons, which has already been described analytically (Wolf and Bortfeld 2012). The effect of such a magnetic field on the delivered dose has been simulated for a magnetic field of 0.5 T and was shown to have a little impact (Raaymakers *et al* 2008). Also the effect of returning electrons (ERE), which is a factor of importance in the MR-linac (Raaijmakers *et al* 2005), is not of importance, because of their low energy (Raaymakers *et al* 2008). However, in the case of a larger magnetic field the dose distribution might change, due to the increasing deflection (Wolf and Bortfeld 2012). Also, this deflection is energy dependent and when using intensity modulated proton therapy (IMPT) plans, a range of proton energies have to be used. This gives rise to the question if a clinically-used magnetic field of 1.5 T will effect the possibility of IMPT planning. If dosimetric feasibility is demonstrated, further research on the technical challenges of a hybrid MRI proton system might be justified.

The aim of this study is to investigate the dosimetric feasibility of IMPT scanning beam proton therapy with the patient placed inside a magnetic field. To fulfill this objective, an infrastructure to generate the proton beamlets needed for the creation of an IMPT plan will be described. Subsequently, the effects of a magnetic field on these beamlets will be investigated and the possibility of IMPT in a magnetic field will be assessed.

First, the behavior of a single proton beam inside a magnetic field is simulated. Second, several IMPT plans are simulated with and without a magnetic field, the properties of which are compared. The basis for the system simulated in this study is a standard 1.5 T MRI system which is integrated with a proton therapy gantry. In this system the direction of the proton beam is perpendicular to the magnetic field direction, so the Lorentz force on proton beam is maximized. While passive beam scattering has been historically the primary modality to deliver proton therapy, pencil beam scanning can provide better conformality, especially at the proximal edge of the target, and reduces neutron scatter (Schneider *et al* 2002). Therefore, it is to be expected that a future hybrid MRI proton therapy system will be based on pencil beam scanning and thus use IMPT, so this technique has been chosen in the simulations. The result of these simulations can not only contribute to dosimetric specifications, but might also lead to some technical specifications of a hybrid MRI proton therapy system.

2. Methods

2.1. Overview

The generation of IMPT plans in a 1.5 T magnetic field is achieved with a home-made, dedicated software infrastructure. The simulations are based on IMPT scanning beam proton therapy. To generate beamlets, the TOol for PArticle Simulation (TOPAS) (Perl *et al* 2012) is used. This software tool for Monte Carlo simulations is based on Geant4 version 9.6.p02 (Allison *et al* 2003, 2006). TOPAS beta version 12 was used for all simulations and the TOPAS default physics list is used.

For the creation of IMPT plans, in-house developed MR-linac Treatment Planning System (MRLTP) (Bol *et al* 2012) is used. This system uses an inverse optimization algorithm to generate IMPT plans (Ziegenhein *et al* 2013).

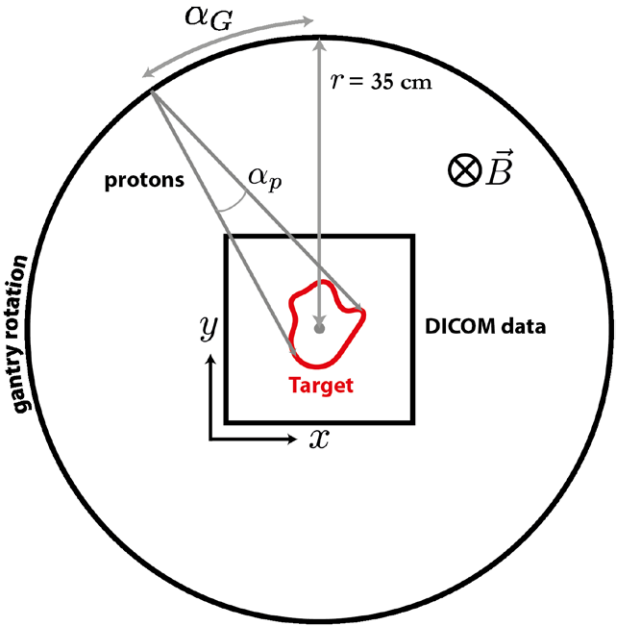

Figure 1. Overview of setup. The dicom data is in the centre, the gantry is placed at a distance r. The gantry angle α_G depends on the location of the target and OARs. For each gantry angle, a range of proton beamlets over the angle α_p are generated, so that the target is completely covered. The magnetic field is in the z-direction.

2.2. Setup

Using TOPAS, the patient DICOM data is read and the Houndsfield units are converted to a density of 1 g cm^{-3} (water) inside and 1.21×10^{-3} g cm^{-3} (air) outside the patient, based on values from the Geant4 Material Database. These data are placed inside a box containing a homogeneous magnetic field. The strength of this field is either 0 T (no magnetic field) or 1.5 T. The direction of the field is in the positive z-direction.

The proton beamlets are placed in the transverse plane at a specified gantry angle. To simulate the effect of proton beam scanning, a range of beamlet angles are simulated from a single gantry angle. For the generation of a complete set of beamlets, the z-direction is traversed to cover the full range of the target. The origin of the protons is placed at 35 cm of the center of the data, which is equal to the MRI bore radius of the MR-linac. Because the angle between the magnetic field lines and the proton beamlet direction is 90°, the proton deflection due to the Lorentz force $\mathbf{F} = \mathbf{v} \times \mathbf{B}$ is maximal. An overview of the setup is shown in figure 1.

The dose distribution is scored in a TOPAS scorer with equal dimensions and number of voxels as the DICOM data.

2.3. Angle and energy

2.3.1. Gantry angles. For each plan three different gantry angles are chosen. This selection is made intuitively, based on the location of the target and the OARs. As shown in figure 1, a range of proton beamlets over an angle α_p are generated. The step size in this range is determined by coverage of the target by the most distal Bragg Peaks. A too large angle step size could lead to insufficient coverage and sub-optimal IMPT plans, while a too small angle

step size will lead to too many beamlets being included in the inverse optimization, leading to a decrease of efficiency. The coverage of the distal side of the target, depends itself on the resolution of the image data (Δx, Δy) and the distance of the gantry r, so the angle α_p can be calculated using

$$\tan \alpha_p = \frac{\min(\Delta x, \Delta y)}{r}, \tag{1}$$

with $\min(\Delta x, \Delta y)$ the smallest resolution in either the x or y direction.

2.3.2. Beamlet energy. An optimal energy step size will give a Bragg Peak in every voxel in the target, so it is directly dependent on the image resolution. The range of a beamlet can be approximated by Bortfeld (1997)

$$R_0 \approx 2.43 \times 10^{-3} E_0^{1.75} \,\mathrm{g\,cm^{-2}}. \tag{2}$$

The range difference per MeV is larger for higher energies, so to determine the energy step size, the highest energy necessary is used. This step size E_{step} is chosen in such a way that

$$R_0^{E_{\max}} - R_0^{E_{\max} - E_{\mathrm{step}}} = \min(\Delta x, \Delta y). \tag{3}$$

2.4. Proton deflection

The radius of the proton follows from the Lorentz force law and is given by

$$r_p = \frac{\sqrt{2Em_p}}{q_p B}, \tag{4}$$

with E the proton energy, m_p the proton mass, q_p the proton charge and B the magnetic field strength. Converting the SI units, this can be approximated as

$$r_p \approx 14.4 \frac{\sqrt{E}}{B}, \tag{5}$$

with the energy in MeV, the magnetic field strength in T and the radius in cm. Figure 2 shows this radius for energies from 3 to 300 MeV.

Because of this curvature, the protons will have deflected from the initial direction when they reach the target. If the distance of the gantry to the body is large and the proton energy is low, the curvature of the protons might even be too large to reach the body. In the former case, the initial direction or angle has to be adjusted so that the Bragg Peak is at the expected location. In the latter case such a correction is no longer possible, but clinically such a situation might not be relevant, because protons with low energies (<70 MeV) are not often used.

To calculate the angle adjustment, it is assumed that the energy loss in air is negligible. Also, the curvature of the beamlet is not taken into consideration in the calculation of the range and thus equation (2) can be used.

The deflection d_p, measured perpendicular to the initial proton direction, can be expressed as

$$d_p \approx r_p \left(1 - \cos\left[\sin^{-1}\left(\frac{d + R_0}{r_p} \right) \right] \right), \tag{6}$$

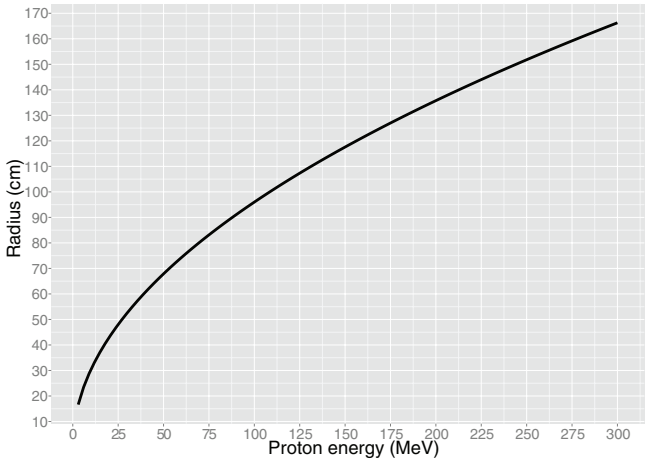

Figure 2. The proton curvature radius as a function of the energy at a magnetic field strength of 1.5 T.

with d the distance from the gantry to the body and R_0 the proton range inside the body. From this, the angle correction γ can be calculated, which is

$$\begin{aligned}\gamma &= \tan^{-1}\left(\frac{d_p}{d+R_0}\right)\\ &= \tan^{-1}\left(\frac{r_p\left(1-\cos\left[\sin^{-1}\left(\frac{d+R_0}{r_p}\right)\right]\right)}{d+R_0}\right).\end{aligned} \tag{7}$$

The deflection for three different distances to body entry is shown in figure 3 and the angle correction is shown in figure 4. The behavior of this function, with a clear minimum, is because of the argument of $\sin^{-1}$, which contains a $E^{1.75}$ in the numerator and a $\sqrt{E}$ in the denominator and the fact that the point of entry in the body is strongly energy dependent.

The gantry angle correction can be applied to either the proton angles or the gantry angles. In both cases, the beamlets will enter the body at a different point and will cross different tissue.

2.5. Data

2.5.1. Beamlet properties. Because of the Lorentz force, the proton beamlets will follow a curved path inside the magnetic field. The Lorentz force law states that the amount of deflection depends on the initial proton energy, the magnetic field strength and the angle between the magnetic field lines and the beam path (cross product). This force might lead to beam widening, because of a dispersion of the proton energies and therefore different curvatures along the beam path. To quantify this, a simulation is done in TOPAS. The setup used is a water phantom of $10\,\text{cm} \times 10\,\text{cm} \times 50\,\text{cm}$ placed inside a magnetic field, which does not extent outside the phantom. Perpendicular to this magnetic field, protons with energies of 50 MeV, 100 MeV, 150 MeV are generated, to cover a broad range of clinical applicable proton energues. The deposited dose is scored in a grid with a voxel size of $1\,\text{mm} \times 1\,\text{mm} \times 10\,\text{mm}$.

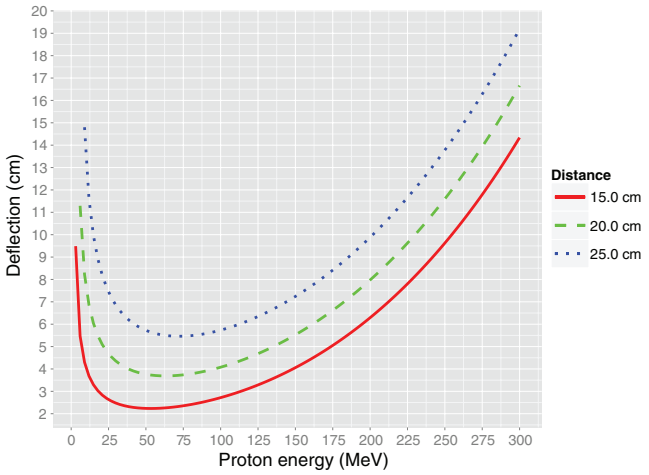

Figure 3. The proton deflection at the location of the Bragg Peak as a function of initial proton energy, for three different distances, at a magnetic field of 1.5 T. The deflection depends on the radius of the curvature. For the lowest energies, the proton beamlet will not reach the body due to a small curvature radius (asymptotic behavior), which in such cases cannot be corrected. Distance = gantry to body distance, Deflection = beamlet deflection at BP location.

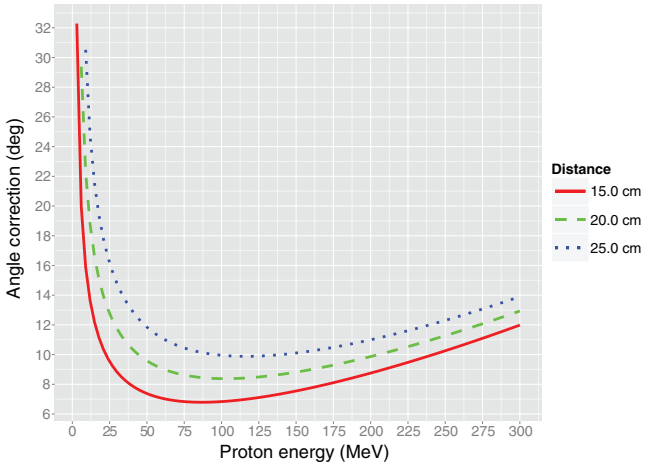

Figure 4. The correction angle γ for a magnetic field of 1.5 T. The initial angle of the the proton beamlet has to be adjusted with this value to get the Bragg Peak at the same location as when no magnetic field is present. Compare with figure 3. Distance = gantry to body distance, Angle correction = γ from equation (7).

For the generation of the IMPT plans, to optimize calculation time of the inverse optimization, a multi-step approach for the beamlet simulation is used. This workflow is schematically shown in figure 5. First, a wide range of beamlets is simulated covering the target. For this simulation run low statistics are used, in total 500 events per beamlet. For the generated beamlets, the location of the Bragg Peak is determined and the beamlets with its Bragg Peak inside the target are identified. For these identified beamlets, a

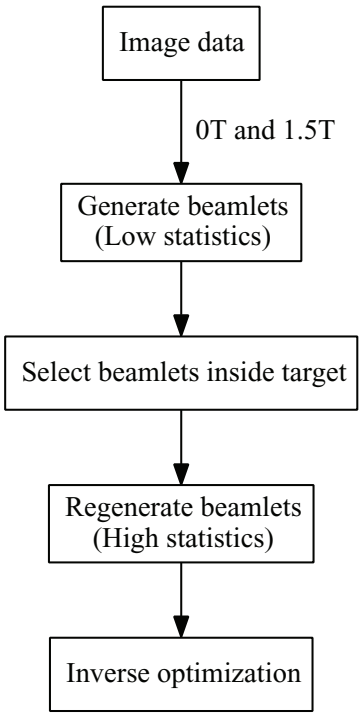

Figure 5. Workflow for the creation of IMPT plans.

second simulation run is done, using high statistics of 10 000 events per beamlet. From this second set of beamlets, the IMPT plans are generated, using the MRLTP. The result is an optimized set of weights for all proton beamlets, from which the dose distribution can be constructed.

2.5.2. DICOM data. Three clinical sites are selected. This selection is based on the depths of their associated targets and their different sizes. The targets are:

1. A shallow head-neck tumor. The depth of the center of the tumor is ∼2 cm. The head-neck region is a challenging site because of the many OARs. The target has a volume of 2.2 cm^3, with a target dose of 25 Gy.
2. A deep head-neck tumor at a depth of ∼5 cm. The target has a volume of 11.0 cm^3, with a target dose of 25 Gy.
3. An artificial, stationary tumor in the liver at a depth of ∼9 cm. The target has a volume of 3.3 cm^3, with a target dose of 25 Gy.

All characteristics of the targets are given in table 1.

2.6. Analysis

The beamlet profiles of the water phantom data are plotted and analyzed using R version 2.15.1 (R Core Team 2012). For the IMPT plans dose parameters are generated using the MRLTP. The dose parameters are analyzed using the aforementioned version of R.

Table 1. Overview of target characteristics and IMPT parameters.

Target	Depth (cm)	Volume (cc)	Resolution (mm)	Energies, ΔE (MeV)	Gantry angles (deg)	$\Delta\alpha_p$ (deg)
HN Shallow	2	2.2	$1.17 \times 1.17 \times 2.0$	15–71, 1	− 25, 0, 25	1
HN Deep	5	11.0	$0.98 \times 0.98 \times 2.0$	95–110, 1	− 35, 0 30	0.15
Liver	9	3.3	$1.0 \times 1.0 \times 1.0$	101–134, 0.5	190, 235, 275	0.2

Note: The depth is of the approximate center of the target, the resolution is of the image data.

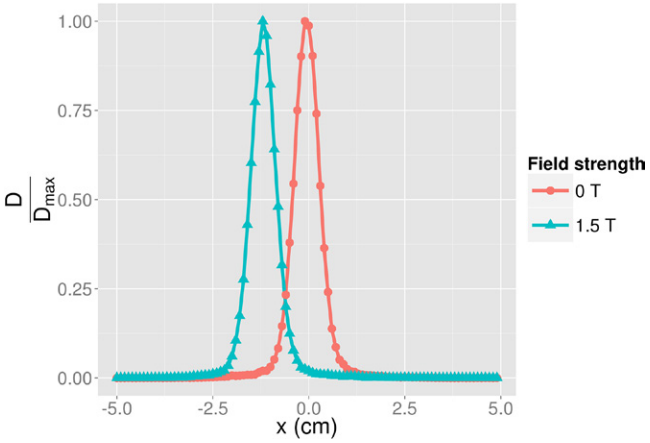

Figure 6. Profiles of the Bragg peaks perpendicular to the beam direction, without and with magnetic field on. The shift of the 1.5 T beam is clearly visible and is 1.14 cm. The width of the fit to the Bragg Peaks is $\sigma = 0.36$ cm for both profiles.

3. Results

3.1. Beamlet generation

Figure 6 shows the profiles of the Bragg Peaks perpendicular to the beam line, both without and with a magnetic field of 1.5 T. The shift of the Bragg Peak inside the magnetic field is clearly visible. Based on a Gaussian fit to the data, this shift is 1.14 cm for 150 MeV. Analytically, the maximum deflection is approximately 1.21 cm (Wolf and Bortfeld 2012), which makes the simulated value consistent with the analytic approximation. The width of the Bragg Peaks is determined by using the same Gaussian fit and is found to be $\sigma = 0.36$ for both Bragg Peaks.

3.2. IMPT plans

3.2.1. Head-Neck shallow. The target is a shallow larynx tumor. Figure 7(a) and (b) show the dose distribution for the 0 T and the 1.5 T IMPT plans. Inside the GTV, the mean dose is 25.3 Gy, with $\sigma = 0.7$ Gy for the 0 T plan and 25.3 Gy, $\sigma = 0.7$ Gy for the 1.5 T plan and thus identical to the 0 T plan. The D95 in the GTV was 24.89 Gy and the dose in all OARs, except the body, was negligible.

Figure 7(c) shows the difference plot of figure 7(a) and (b). The absolute difference inside the target is shown in the histogram of figure 7(d). The mean of the difference is 0.018 Gy, with a standard deviation of $\sigma = 0.65$ Gy. While outside of the target a clear difference is

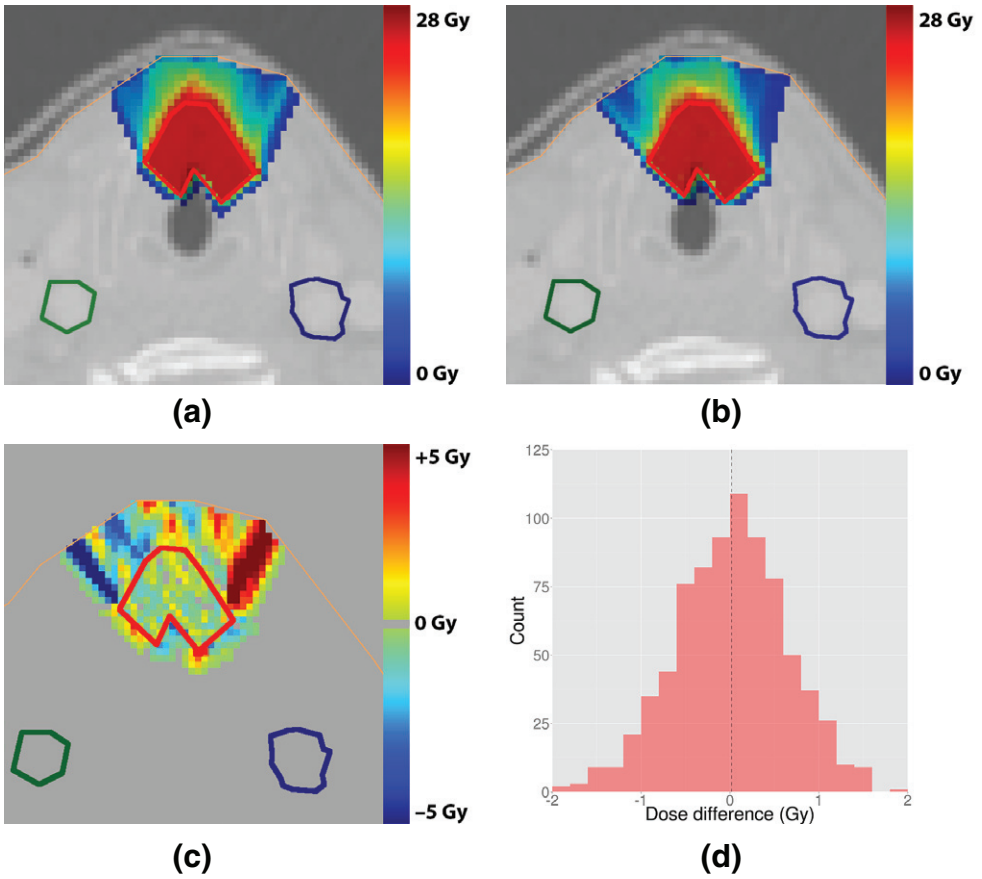

Figure 7. Head-Neck shallow plan. Dose distribution in transversal plane for 0 T and 1.5 T IMPT plan shown contours: GTV (red), left carotid artery (blue), right carotid artery (green). (a) 0 T. (b) 1.5 T. (c) Absolute dose difference in transversal plane, which is the difference between figure 7(a) and (b). (d) Histogram of the dose difference inside the GTV. Mean value is 0.018 Gy ($\sigma = 0.65$ Gy), shown by the dashed line. The bin size is 0.2 Gy.

visible, it is minor inside the target. The former can be attributed to the fact that the optimizer selects different beamlets in the case with a magnetic field, because of the curvature.

3.2.2. Head-Neck deep. The target is a deep larynx tumor. Figure 8(a) and (b) show the dose distribution for the 0 T and the 1.5 T plans. Inside the CTV, the mean dose is $\mu = 26.21$ Gy, with $\sigma = 1.51$ Gy for the 0 T plan and $\mu = 26.37$ Gy, $\sigma = 1.52$ Gy for the 1.5 T plan. To quantify the difference in dose distribution, the dose difference plot is shown is figure 8(c). The absolute difference inside the target is shown in the histogram of figure 8(d). The mean of the difference is −0.17 Gy, with $\sigma = 1.11$ Gy.

3.2.3. Liver. In this plan, the target is an artificial target deep in the liver. The constraints on the OARs are taken from Chang *et al* (2009), based on their treatment of patients with unresectable adenocarcinoma. Figure 9(a) and (b) shows the dose distribution for the 0 T and

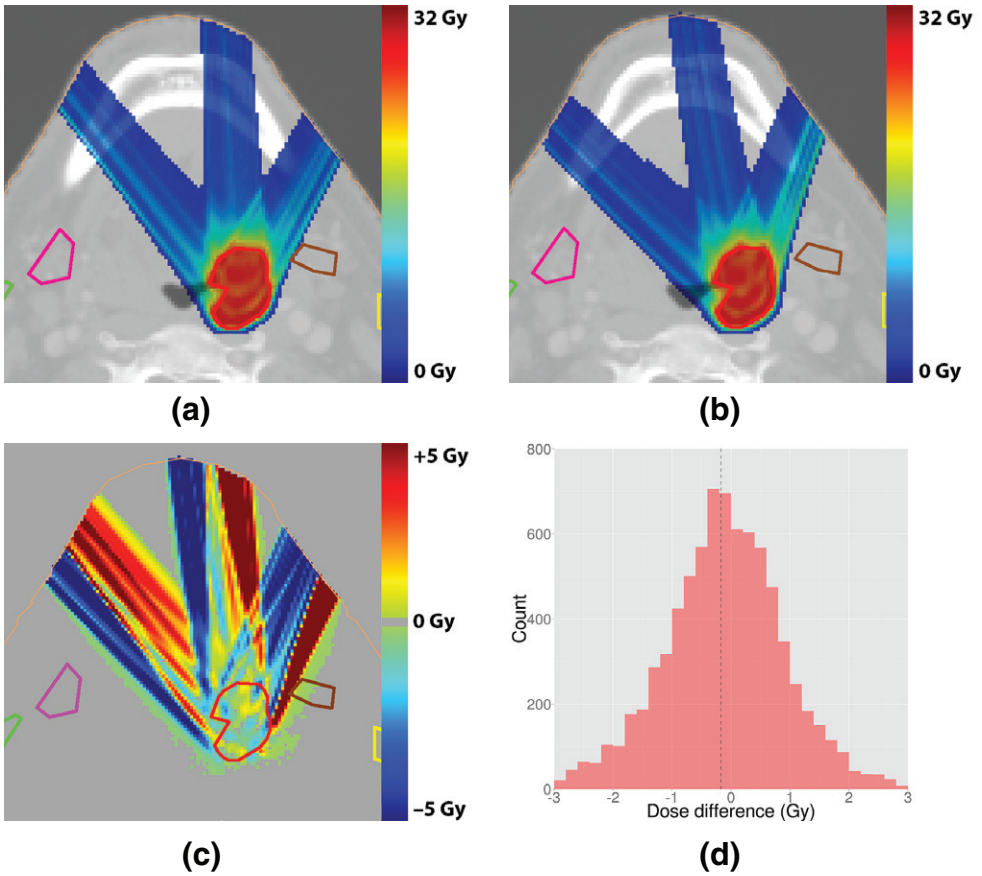

Figure 8. Head-Neck deep plan. Dose distribution in transversal plane for 0 T and 1.5 T IMPT plan and the dose difference between the two plans. Shown contours: target (red), left submandibular gland (brown), right submandibular gland (purple), left parotid gland (yellow), right parotid gland (green). (a) 0 T. (b) 1.5 T. (c) Absolute dose difference in transversal plane, which is the difference between figure 8(a) and (b). (d) Histogram of the dose difference inside the GTV. Mean value is −0.17 Gy ($\sigma = 1.11$ Gy), shown by the dashed line. The bin size is 0.2 Gy.

the 1.5 T plans. Inside the GTV, the mean dose is 25.5 Gy ($\sigma = 1.25$ Gy) for the 0 T plan and 25.9 Gy ($\sigma = 1.21$ Gy) for the 1.5 T plan. The dose difference plot is shown in figure 9(c). The absolute difference inside the target is shown in the histogram of figure 9(d). The mean of the difference is −0.34 Gy, with a standard deviation of $\sigma = 0.62$ Gy.

3.3. Summary

Based on the results in the previous sections, it is possible to generate IMPT plans using the described framework, with and without a magnetic field. The only impact of the magnetic field on the IMPT plans is the selection of a different set of beamlets, because of the proton curvature. All sets of selected beamlets have their Bragg Peaks inside the target and can be used to calculate a combination of weights which will deliver the desired dose inside the target, while meeting the dose constraints of the OARs.

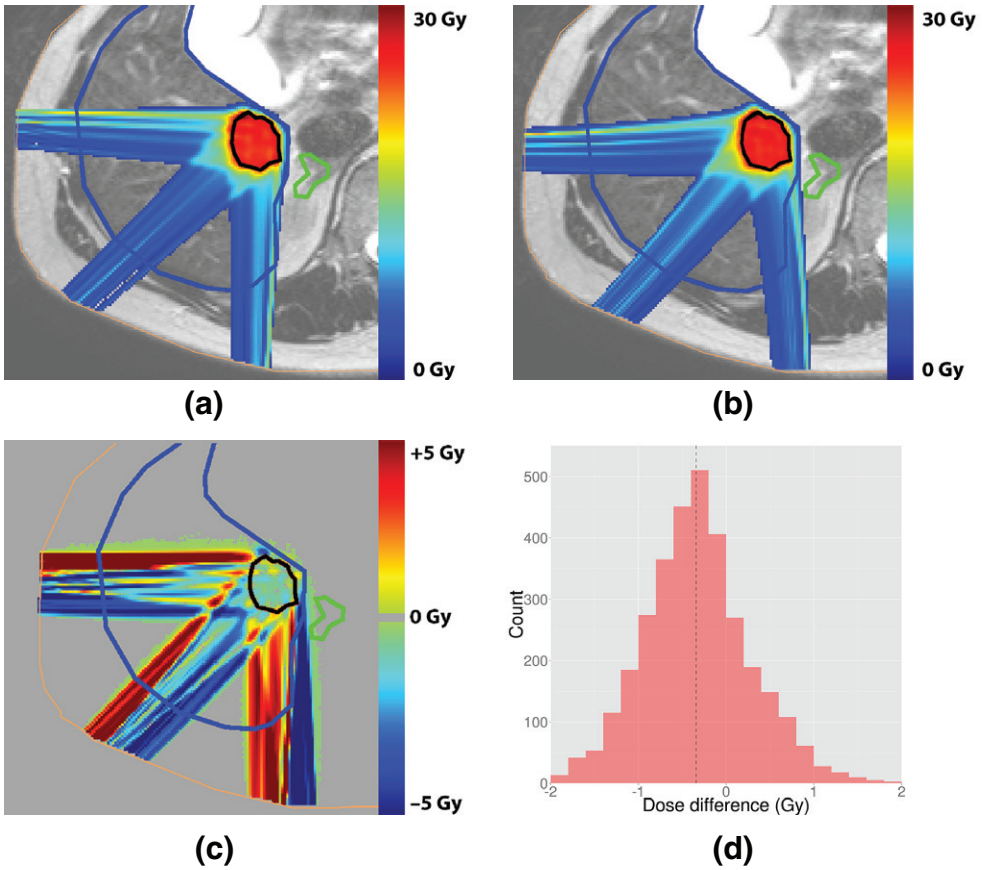

Figure 9. Liver plan. Dose difference between 0 T and 1.5 T IMPT plan. Shown contours: GTV (black), liver (blue), right adrenal (green). (a) 0 T. (b) 1.5 T. (c) Absolute dose difference in transversal plane, which is the difference between figure 9(a) and (b). (d) Histogram of the dose difference inside the GTV. Mean value is -0.34 Gy ($\sigma = 0.62$ Gy), shown by the dashed line. The bin size is 0.2 Gy.

For the shallow target, the difference in beamlet selection is small. For deeper targets, it is clear that the proton curvature plays a larger role. If there are OARs close to the proton beamlet path, the set of beamlets inside a magnetic field might pass through such an OAR, while the set without a magnetic field did not. This is something which should be taken into consideration in the case of deeper tumors and it might be necessary to incorporate this when optimizing the gantry angles.

4. Discussion

In this study, several assumptions and simplifications are made. The number of gantry angles and thus the fields for each IMPT plan was chosen to be three. There is a trade-off between delivering a homogeneous dose distribution and limiting the number of fields to spare organs at risk. Selecting three fields seems to be an advantageous choice (Steneker *et al* 2006), nevertheless there might be a rationale for a different number of fields. Because there was no major

impact of the magnetic field on any IMPT plan, it is assumed that an increase in the number of fields will not affect the results as presented here.

The same argument can be made for the selection of the gantry angles. The angles were selected in such a way to spare OARs as much as possible, which was determined by visual analysis of the image data. The angles could probably be optimized, but it is assumed that this will not affect the results in a negative way.

The material inside the body was set to a density of 1 g cm^{-3}. Although this value is close to the densities of both muscle and adipose tissue, the effects of for example bone and air cavities are not taken into account. Such effects might influence the energy loss of the proton beamlets and thus the dose distribution inside the body, but the ERE will still be of no influence. Since only the beamlets with a simulated Bragg Peak inside the target are selected, this simplification should not influence the optimization. Setting the densities to the physical densities will produce a different set of beamlets for the optimization, but should give a plan with a similar dose distribution in the target.

Another factor in the simulation of beamlets, are the stopping powers of materials. By using a single density, this problem is mostly avoided. Still, in clinical practice the stopping powers play an important role. Because MR can provide better tissue characterization compared with other image modalities, especially for soft tissue, it could be argued that the stopping power determination will benefit from the use of this imaging modality. Nevertheless, the conversion of MR data to correct stopping powers is not trivial (Rank *et al* 2013a, 2013b), and might make an increase of the margin around the target necessary.

The correction of the proton deflection is an approximation, which seems appropriate for the used resolution and energies. For low energies, the correction angle can be quite large or there might even be no correction possible. Another solution for lower energies, is to place tissue-equivalent material on the patient to absorb the excess of energy. In such a setup the deflection between the gantry angle and the body can be reduced.

Because of the bore radius of 35 cm of the MR-linac, this gantry distance has also been chosen for the simulations in this study. Nevertheless, this is a somewhat arbitrary choice. The deflection at the target is dependent on this distance, however, if a correction is applied, the gantry distance should not influence the presented results.

Three sites were selected for this study. This selection has been based on (1) the complexity of the site, with for example many OARs in the Head-Neck sites (2) different location of the sites, and (3) the different size of the targets. The optimization method which is used, produces the plans based on provided constraints. Therefore, it can be expected that this method will work for any site, as long as a correct set of proton beamlets can be provided as input.

In the generation of the beamlets inside a magnetic field, the initial angle of the beamlets is adjusted based on a calculated angle correction. In this calculation, it is assumed that the body consists of homogeneous material, in the case of these simulations water. When the true stopping powers of the body material are taken into account, this angle correction has to be adjusted to incorporate the difference in energy loss, range and curvature.

The framework for simulations enables comparisons for different treatment modalities and planning systems.

5. Conclusion

This study shows that the generation of an IMPT plan in a magnetic field is feasible. The presented framework based on the Monte Carlo simulation of proton beamlets, combined with the use of an inverse optimization method, can be used to produce IMPT scanning beam plans.

It also shows the dosimetric feasibility of IMPT in a transverse magnetic field of 1.5 T. Using the simulated proton beamlets, it is possible to create IMPT scanning beam plans for several sites. All these plans meet the clinical constraints for the dose to the target and the OARs. The impact of the magnetic field is only the curvature of the beamlets, which means that in certain cases an OAR might get a different dose due to this curvature. This issue is mainly observed in deeper targets and should in such situations be taken into consideration. The chosen setup of a 1.5 T magnetic field perpendicular to the proton path gives the largest curvature of protons and can therefore be considered the worst case scenario. It can therefore be concluded that there are no dosimetric obstacles for such a system, when an MRI with this field strength (or lower) is used.

This study is based on simulations and not on any hardware implementation, due to the fact that at the moment there is no hybrid MRI proton therapy system available. The conclusion on the technical specifications is that the magnetic field does not hamper the employment of IMPT.

Acknowledgments

We would like to thank the TOPAS developers and J Perl in particular for helping us by providing the features in the software we needed to get our framework working.

References

Allison J *et al* 2003 Geant4—a simulation toolkit *Nucl. Instrum. Methods Phys. Res.* **506** 250–303
Allison J *et al* 2006 Geant4 developments and applications *IEEE Trans. Nucl. Sci.* **53** 270–8
Bol G H, Hissoiny S, Lagendijk J J W and Raaymakers B W 2012 Fast online Monte Carlo-based IMRT planning for the MRI linear accelerator *Phys. Med. Biol.* **57** 1375–85
Bortfeld T 1997 An analytical approximation of the Bragg curve for therapeutic proton beams *Med. Phys.* **24** 2024–33
Brenner D J and Hall E J 2007 Computed tomography: an increasing source of radiation exposure *New Engl. J. Med.* **357** 2277–84
Chang D T, Schellenberg D, Shen J, Kim J, Goodman K A, Fisher G A, Ford J M, Desser T, Quon A and Koong A C 2009 Stereotactic radiotherapy for unresectable adenocarcinoma of the pancreas *Cancer* **115** 665–72
Chen W, Unkelbach J, Trofimov A, Madden T, Kooy H, Bortfeld T and Craft D 2012 Including robustness in multi-criteria optimization for intensity-modulated proton therapy *Phys. Med. Biol.* **57** 591
Fallone B G 2014 The rotating biplanar linac–magnetic resonance imaging system *Semin. Radiat. Oncol.* **24** 200–2
Glimelius B, Blomquist E, Grusell E, Jung B Montelius A and Isacsson U 1999 Potential gains using high-energy protons for therapy of malignant tumours *Acta Oncol.* **38** 137–45
Keall P J, Barton M and Crozier S 2014 The Australian magnetic resonance imaging–linac program *Semin. Radiat. Oncol.* **24** 203–6
Liu W, Frank S J, Li X, Li Y, Park P C, Dong L, Zhu X R and Mohan R 2013 Effectiveness of robust optimization in intensity-modulated proton therapy planning for head and neck cancers *Med. Phys.* **40** 051711
Liu W, Zhang X, Li Y and Mohan R 2012 Robust optimization of intensity modulated proton therapy *Med. Phys.* **39** 1079–91
Lomax A J 2008 Intensity modulated proton therapy and its sensitivity to treatment uncertainties 1: the potential effects of calculational uncertainties *Phys. Med. Biol.* **53** 1027
Mackie T R *et al* 2003 Image guidance for precise conformal radiotherapy *Int. J. Radiat. Oncol. Biol. Phys.* **56** 89–105
Mock U, Georg D, Bogner J, Auberger T and Pötter R 2004 Treatment planning comparison of conventional, 3D conformal, and intensity-modulated photon (IMRT) and proton therapy for paranasal sinus carcinoma *Int. J. Radiat. Oncol. Biol. Phys.* **58** 147–54

Nguyen N P *et al* 2013 Potential applications of imaging and image-guided radiotherapy for brain metastases and glioblastoma to improve patient quality of life *Front. Oncol.* **3** 284
Paganetti H (ed) 2012a *Proton Therapy Physics* (*Series in Medical Physics and Biomedical Engineering*) (Boca Raton, FL: CRC Press)
Paganetti H 2012b Range uncertainties in proton therapy and the role of Monte Carlo simulations *Phys. Med. Biol.* **57** R99
Park P C, Zhu X R, Lee A K, Sahoo N, Melancon A D, Zhang L and Dong L 2012 A beam-specific planning target volume (PTV) design for proton therapy to account for setup and range uncertainties *Int. J. Radiat. Oncol. Biol. Phys.* **82** e329–36
Perl J, Shin J, Schumann J, Faddegon B and Paganetti H 2012 TOPAS: an innovative proton Monte Carlo platform for research and clinical applications *Med. Phys.* **39** 6818–37
Raaijmakers A J E, Raaymakers B W and Lagendijk J J W 2005 Integrating a MRI scanner with a 6 MV radiotherapy accelerator: dose increase at tissue-air interfaces in a lateral magnetic field due to returning electrons *Phys. Med. Biol.* **50** 1363–76
Raaymakers B W *et al* 2009 Integrating a 1.5 T MRI scanner with a 6 MV accelerator: proof of concept *Phys. Med. Biol.* **54** N229–37
Raaymakers B W, Raaijmakers A J E and Lagendijk J J W 2008 Feasibility of MRI guided proton therapy: magnetic field dose effects *Phys. Med. Biol.* **53** 5615–22
Rank C M, Hünemohr N, Nagel A M, Röthke M C, Jäkel O and Greilich S 2013a MRI-based simulation of treatment plans for ion radiotherapy in the brain region *Radiother. Oncol.* **109** 414–8
Rank C M, Tremmel C, Hünemohr N, Nagel A M, Jäkel O and Greilich S 2013b MRI-based treatment plan simulation and adaptation for ion radiotherapy using a classification-based approach *Radiat. Oncol.* **8** 51
R Core Team 2012 *R: a Language and Environment for Statistical Computing (R Foundation for Statistical Computing Vienna, Austria)* (www.R-project.org)
Schepper A M D, Beuckeleer L D, Vandevenne J and Somville J 2000 Magnetic resonance imaging of soft tissue tumors *Eur. Radiol.* **10** 213–223
Schneider Y, Agosteo S, Pedroni E and Besserer J 2002 Secondary neutron dose during proton therapy using spot scanning *Int. J. Radiat. Oncol. Biol. Phys.* **53** 244–51
Semelka R C, Armao D M, Elias J and Huda W 2007 Imaging strategies to reduce the risk of radiation in CT studies, including selective substitution with MRI *J. Magn. Reson. Imaging* **25** 900–9
Steneker M, Lomax A and Schneider U 2006 Intensity modulated photon and proton therapy for the treatment of head and neck tumors *Radiother. Oncol.* **80** 263–7
Suit H *et al* 2003 Proton beams to replace photon beams in radical dose treatments *Acta Oncol.* **42** 800–8
Trofimov A, Nguyen P L, Coen J J, Doppke K P, Schneider R J, Adams J A, Bortfeld T R, Zietman A L, DeLaney T F and Shipley W U 2007 Radiotherapy treatment of early-stage prostate cancer with IMRT and protons: a treatment planning comparison *Int. J. Radiat. Oncol. Biol. Phys.* **69** 444–53
Unkelbach J, Bortfeld T, Martin B C and Soukup M 2009 Reducing the sensitivity of IMPT treatment plans to setup errors and range uncertainties via probabilistic treatment planning *Med. Phys.* **36** 149–63
Unkelbach J, Chan T C Y and Bortfeld T 2007 Accounting for range uncertainties in the optimization of intensity modulated proton therapy *Phys. Med. Biol.* **52** 2755
Wolf R and Bortfeld T 2012 An analytical solution to proton Bragg Peak deflection in a magnetic field *Phys. Med. Biol.* **57** N329–37
Ziegenhein P, Kamerling C P, Bangert M, Kunkel J and Oelfke U 2013 Performance-optimized clinical IMRT planning on modern CPUs *Phys. Med. Biol.* **58** 3705–15